Coupling of Circumferential Modes in a Circular Plate

Jie Pan (1), Dave Matthews (1), and Jacob Ibrahim (1)

(1) The University of Western Australia, WA 6009, Australia

Abstract - Unlike the vibrational modes of a circular plate with a perfectly clamped boundary condition, the characteristics of circular plates in practical scenarios are influenced by the clamping pressure at the boundary. In this paper, we explore how the natural frequencies of degenerated non-axial symmetric modes are shifted and split. These phenomena are explained by the coupling between circumferential modes, which is induced by non-uniform boundary conditions.

1 INTRODUCTION

An understanding of the vibration characteristics of a circular plate is a basic requirement for studying the structural vibration under static and dynamic fluid loading [1,2], as well as vibration-induced Faraday waves and droplet generation via surface fracture [3,4]. Discrepancies are often observed between the measured frequency response of circular plates clamped by heavy flanges and the predictions of thin plate theory with ideal clamped boundary conditions [5]. Typical discrepancies are the decrease of natural frequencies from the predicted values of the clamped plate and a splitting of the natural frequencies of the originally degenerated cosine and sine modes. Since theoretical 'clamped boundary' conditions are nearly impossible to replicate in laboratory settings, it is necessary to understand the mechanisms involved in the changes in the plate characteristics caused by more realistic boundary conditions and to develop an appropriate model for this understanding.

The change in the natural frequencies of the plate modes due to the imperfect clamping by the flanges may be explained by considering the characteristics of a mass-spring oscillator supported by boundary stiffness (K_2) and inertia (M_2) as shown in Figure 1. The natural frequency of the oscillator is related to the stiffness ratio $r_K = \frac{K_2}{K_1}$ and mass ratio $r_M = \frac{M_2}{M_1}$ by:

$$\tilde{f}_n = f_n \sqrt{\frac{\frac{r_K}{1+r_K}}{\frac{r_M}{1+r_M}}}, \tag{1}$$

where $f_n = \frac{1}{2\pi}\sqrt{\frac{K_1}{M_1}}$ is the natural frequency of the oscillator with perfectly clamped boundary condition. This result demonstrates that that if $r_M = \infty$, $\tilde{f}_n$ reduces from f_n as r_K reduces from infinity. If $r_K = \infty$, $\tilde{f}_n$ increases from f_n as r_M reduces from infinity. It also indicates that the reduction of natural frequencies in the flanged circular plate is caused by non-sufficient boundary stiffness and clamping pressure.

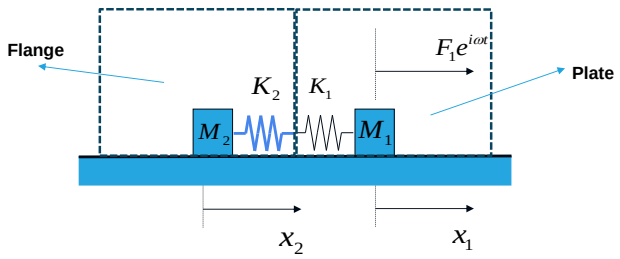

Figure 1 – Illustration model for the shift of natural frequency of an oscillator by its boundary conditions.

The modal characteristics of a circular plate with non-uniform boundary stiffness are derived analytically in this paper. An example of a non-uniform boundary condition is a flange clamped by bolts at discrete angular locations. We demonstrate that insufficient boundary stiffness causes the reduction in natural frequencies. The coupling of circumferential modes in the plate via non-uniform boundary stiffness causes the splitting of the natural frequencies of originally degenerate circumferential modes.

2 MODEL OF A CIRCULAR PLATE

The displacement, $w(\vec{\sigma},t)=We^{i\omega t}$, of a thin plate is described by:

$$(-\rho h\omega^2+D\nabla^4)W=0 \tag{2}$$

where $D=\frac{Eh^3}{12(1-\nu^2)}$, ρ, E, ν and h are the bending stiffness, density, Young's modulus Poisson ratio and thickness of the plate. Non-uniform boundary conditions introduces plate asymmetry, and the displacement can be expended as [6]:

$$W(\vec{\sigma},\omega)=\sum_{n,m}\cos(n\theta)R_{Cn}(kr)+\sum_{n,m}\sin(n\theta)R_{Sn}(kr) \tag{3}$$

where $\begin{bmatrix}R_{Cn}(kr)\\R_{Sn}(kr)\end{bmatrix}=\begin{bmatrix}A_{Cn}J_n(kr)+C_{Cn}I_n(kr)\\A_{Sn}J_n(kr)+C_{Sn}I_n(kr)\end{bmatrix}$, $k=(\frac{\omega^2\rho h}{D})^{1/4}$ and $\vec{\sigma}=(r,\theta)$. In this analysis, the non-uniform boundary is modelled by springs with a torsional stiffness $K_\psi(\theta)$ and only non-zero angular displacement is allowed at the boundary. Thus, the boundary conditions at $r=a$ are:

$$M_r(a,\theta)=K_\psi(\theta)\frac{\partial W}{\partial r}(a,\theta) \text{ and} \tag{4}$$

$$W(a,\theta)=0, \tag{5}$$

where bending moment is related to the plate displacement by:

$$M_r=-D[\frac{\partial^2 W}{\partial r^2}+\nu(\frac{1}{r}\frac{\partial W}{\partial r}+\frac{1}{r^2}\frac{\partial^2 W}{\partial\theta^2})]. \tag{6}$$

The angular-dependent stiffness can be represented using the Fourier series:

$$K_\psi(\theta)=\sum_p K_{\psi Cp}\cos(p\theta)+\sum_p K_{\psi Sp}\sin(p\theta). \tag{7}$$

Substituting the displacement (Equation (3)) and boundary stiffness (Equation (7)) into Equation (4) results in the modal equation describing the bending moment in terms of the plate displacement:

$$\begin{bmatrix}M_{rCs}\\M_{rSs}\end{bmatrix}=\int_0^{2\pi}\begin{bmatrix}\cos(s\theta)\\\sin(s\theta)\end{bmatrix}M_r(a,\theta)d\theta=\int_0^{2\pi}\begin{bmatrix}\cos(s\theta)\\\sin(s\theta)\end{bmatrix}K_\psi(\theta)\frac{\partial W}{\partial r}(a,\theta)d\theta \text{ and} \tag{8}$$

the boundary condition in Equation (5) leads to:

$$\begin{bmatrix}R_{Cs}(\lambda) & R_{Ss}(\lambda)\end{bmatrix}^T=0, \tag{9}$$

where $\lambda = ka$. Because of non-uniform stiffness, the right-hand side of Equation (8) processes weighted modal coupling integrals, which describe the coupling between the s^{th} circumferential modes ($\begin{bmatrix}\cos(s\theta)\\ \sin(s\theta)\end{bmatrix}$) and the n^{th} circumferential modes ($\begin{bmatrix}\cos(n\theta)\\ \sin(n\theta)\end{bmatrix}$) weighted by the p^{th} stiffness components ($\begin{bmatrix}\cos(p\theta)\\ \sin(p\theta)\end{bmatrix}$). Eight integrals, containing the coupling coefficients between circumferential modes, are presented in the following two (2×2) matrices:

$$\Pi_{Cs}^{np} = \int_0^{2\pi} \cos(s\theta) \begin{bmatrix}\cos(n\theta)\\ \sin(n\theta)\end{bmatrix} \begin{bmatrix}\cos(p\theta)\\ \sin(p\theta)\end{bmatrix}^T d\theta \text{ and,} \tag{10}$$

$$\Pi_{Ss}^{np} = \int_0^{2\pi} \sin(s\theta) \begin{bmatrix}\cos(n\theta)\\ \sin(n\theta)\end{bmatrix} \begin{bmatrix}\cos(p\theta)\\ \sin(p\theta)\end{bmatrix}^T d\theta . \tag{11}$$

The orthogonal property of the weighted modal coupling integrals in Equations (10) and (11) is analysed (see Appendix) based on their symmetrical properties in $0 \le \theta \le 2\pi$, which leads to the following results. The axial symmetric mode ($s = 0$), couples with all $\cos(n\theta)$ and $\sin(n\theta)$ modes ($n > 0$) via the stiffness components in the following modal boundary condition:

$$M_{rC0} = \frac{\lambda}{a}\{K_{\psi C0} R_{C0}^{'}(\lambda)\Lambda_{C00} + \sum_{n=1}^{N}[K_{\psi Cn} R_{Cn}^{'}(\lambda)\Lambda_{Cnn} + K_{\psi Sn} R_{Sn}^{'}(\lambda)\Lambda_{Snn}]\} \tag{12}$$

where $\Lambda_{Cnn} = \begin{cases} 2\pi & n = 0 \\ \pi & n > 0 \end{cases}$ and $\Lambda_{Snn} = \pi$. The cosine mode, $\cos(s\theta)$, $s > 0$, only couples with $n = s$ cosine mode via $p = 0$ stiffness component and with $n = 0$ mode via $p = s$ cosine stiffness component:

$$M_{rCs} = \frac{\lambda}{a}[K_{\psi C0} R_{Cs}^{'}(\lambda)\Lambda_{Css} + K_{\psi Cs} R_{C0}^{'}(\lambda)\Lambda_{Css}] . \tag{13}$$

Similarly, the sine mode, $\sin(s\theta)$ and $s > 0$, only couples with the $n = s$ sine mode via $p = 0$ stiffness component and with $n = 0$ mode via $p = s$ sine stiffness component:

$$M_{rSs} = \frac{\lambda}{a}[K_{\psi C0} R_{Ss}^{'}(\lambda)\Lambda_{Sss} + K_{\psi Ss} R_{C0}^{'}(\lambda)\Lambda_{Sss}] . \tag{14}$$

Together with Equation (9), Equations (12) to (14) form the eigen-equation of the circular plate with non-uniform torsional boundary stiffness. If the boundary stiffness is uniform, $K_{\psi}(\theta) = K_{\psi C0}$, then the circumferential modes are uncoupled. The cosine and sine circumferential modes with the same mode number are degenerate and have the same natural frequency. The natural frequency of each mode increases as the boundary stiffness decreases, approaching the natural frequency of the same plate with clamped boundary condition when the boundary stiffness becomes infinity.

To illustrate the property of coupled circumferential modes, we consider a boundary condition consisting of a uniform $K_{\psi C0}$ and a cosine stiffness component $K_{\psi Cp}\cos(p\theta)$ for $p \ne 0$:

$$K_{\psi}(\theta) = K_{\psi C0} + K_{\psi Cp}\cos(p\theta). \tag{15}$$

For this case, only the $s = 0$ and $\cos(p\theta)$ modes are coupled, resulting in the modal coupling equations:

$$M_{rC0} = \frac{\lambda}{a}[K_{\psi C0}R'_{C0}(\lambda)\Lambda_{C00} + K_{\psi Cp}R'_{Cp}(\lambda)\Lambda_{Cpp}] \text{ and} \tag{16a}$$

$$M_{rCp} = \frac{\lambda}{a}[K_{\psi C0}R'_{Cp}(\lambda)\Lambda_{Cpp} + K_{\psi Cp}R'_{C0}(\lambda)\Lambda_{Cpp}]. \tag{16b}$$

Substituting Equation (3) into Equation (6), Equation (16) is expressed in terms of the coefficients of the two circumferential modes:

$$A_{C0}\hat{M}_{AC0}(\lambda) + C_{C0}\hat{M}_{CC0}(\lambda) = A_{Cp}\hat{\Omega}_{ACp}(\lambda) + C_{Cp}\hat{\Omega}_{CCp}(\lambda) \text{ and} \tag{17a}$$

$$A_{Cp}\hat{M}_{ACp}(\lambda) + C_{Cp}\hat{M}_{CCp}(\lambda) = A_{C0}\hat{\Omega}_{AC0}(\lambda) + C_{C0}\hat{\Omega}_{CC0}(\lambda) \tag{17b}$$

where the non-dimensional modal bending moments and angular displacements are:

$$\hat{M}_{AC0}(\lambda) = \left\{[J_2(\lambda) - J_0(\lambda)] - \frac{2}{\lambda}[\nu + S_{R0}]J_1(\lambda)\right\}, \tag{18a}$$

$$\hat{M}_{CC0}(\lambda) = \left\{[I_2(\lambda) + I_0(\lambda)] + \frac{2}{\lambda}[\nu + S_{R0}]I_1(\lambda)\right\}, \tag{18b}$$

$$\hat{M}_{ACp}(\lambda) = \left\{[J_{p+2}(\lambda) + J_{p-2}(\lambda)] - \frac{2}{\lambda}[\nu + S_{R0}][J_{p+1}(\lambda) - J_{p-1}(\lambda)] - [2 + \frac{4\nu p^2}{\lambda^2}]J_p(\lambda)\right\}, \tag{18c}$$

$$\hat{M}_{CCp}(\lambda) = \left\{[I_{p+2}(\lambda) + I_{p-2}(\lambda)] + \frac{2}{\lambda}[\nu + S_{R0}][I_{p+1}(\lambda) + I_{p-1}(\lambda)] + (2 - \frac{4\nu p^2}{\lambda^2})I_p(\lambda)\right\}, \tag{18d}$$

$$\hat{\Omega}_{AC0}(\lambda) = -4S_{RCp}J'_0(\lambda), \hat{\Omega}_{CC0}(\lambda) = -4S_{RCp}I'_0(\lambda) \text{ and} \tag{19a,b}$$

$$\hat{\Omega}_{ACp}(\lambda) = -S_{RCp}J'_p(\lambda), \ \hat{\Omega}_{CCp}(\lambda) = -S_{RCp}I'_p(\lambda) \tag{19c,d}$$

where $S_{R0} = \frac{K_{\psi C0}a}{D}$ and $S_{RCp} = \frac{K_{\psi Cp}a}{D}$ are stiffness ratios. Combining Equation (9) for $s = 0$ and $s = p$ modes:

$$\begin{bmatrix} A_{C0}J_0(\lambda) + C_{C0}I_0(\lambda) & A_{Cp}J_p(\lambda) + C_{Cp}I_p(\lambda) \end{bmatrix}^T = 0, \tag{20}$$

results in the eigen equations of the coupled $s = 0$ and $s = p$ cosine circumferential modes. Other circumferential modes are uncoupled, and their eigenvalue solution is a straightforward problem.

3 PROPERTY OF COUPLED CIRCUMFERENCIAL MODES

3.1 Modal Characteristics

If $K_{\psi C0} = \infty$ and $K_{\psi Cp} = 0$, the plate is clamped. This condition is satisfied by letting the right-hand side of Equation (17) being zero. Combined with Equation (20), the eigen-equation for $s = 0$ or $s = p$ cosine mode is:

$$I_s(\lambda)\hat{\Omega}_{ACs}(\lambda) - J_s(\lambda)\hat{\Omega}_{CCs}(\lambda) = 0\,, \tag{21}$$

yielding the m^{th} eigenvalue λ_{sm} for the s^{th} circumferential modes and mode shape function:

$$\phi_{Cs,m}(\vec{\sigma}) = \cos(s\theta)\hat{R}_{Cs}(\frac{\lambda_{sm}}{a}r) \quad \text{and} \tag{22}$$

where $\lambda_{sm} = k_{sm}a$ and the natural frequency of the $(s,m)^{th}$ mode is:

$$\omega_{sm} = \sqrt{\frac{D}{\rho h}}k_{sm}^2 = \sqrt{\frac{D}{\rho h}}(\frac{\lambda_{sm}}{a})^2\,. \tag{23}$$

As $C_{Cs} = -A_{Cs}\dfrac{J_s(\lambda_{sm})}{I_s(\lambda_{sm})}$ based on Equation (20),

$$\hat{R}_{Cs}(\frac{\lambda_{sm}}{a}r) = J_s(\frac{\lambda_{sm}}{a}r) - \frac{J_s(\lambda_{sm})}{I_s(\lambda_{sm})}I_s(\frac{\lambda_{sm}}{a}r)\,. \tag{24}$$

If $K_{\psi C0} \neq 0$ and $K_{\psi Cp} = 0$, the eigen equation for $s = 0$ and $s = p$ modes becomes:

$$I_s(\lambda)\hat{M}_{ACs}(\lambda) - J_s(\lambda)\hat{M}_{CCs}(\lambda) = 0 \tag{25}$$

resulting in the m^{th} eigenvalue of the s^{th} circumferential mode. The mode shape function takes the same form as in Equation (22) with the radial component of:

$$\hat{R}_{Cs}(\frac{\lambda_{sm}}{a}r) = J_s(\frac{\lambda_{sm}}{a}r) - \frac{\hat{M}_{ACs}(\lambda_{sm})}{\hat{M}_{CCs}(\lambda_{sm})}I_s(\frac{\lambda_{sm}}{a}r)\ . \tag{26}$$

If $K_{\psi C0} \neq 0$ and $K_{\psi Cp} \neq 0$, Equation (17) is simplified by using Equation (20) as:

$$A_{C0}[\hat{M}_{AC0}(\lambda) - \frac{J_0(\lambda)}{I_0(\lambda)}\hat{M}_{CC0}(\lambda)] - A_{Cp}[\hat{\Omega}_{ACp}(\lambda) - \frac{J_p(\lambda)}{I_p(\lambda)}\hat{\Omega}_{CCp}(\lambda)] = 0 \quad \text{and} \tag{27a}$$

$$A_{C0}[\hat{\Omega}_{AC0}(\lambda) - \frac{J_0(\lambda)}{I_0(\lambda)}\hat{\Omega}_{CC0}(\lambda)] - A_{Cp}[\hat{M}_{ACp}(\lambda) - \frac{J_p(\lambda)}{I_p(\lambda)}\hat{M}_{CCp}(\lambda)] = 0\,, \tag{27b}$$

resulting in the eigen equation for the coupled $s = 0$ and $s = p$ cosine circumferential modes:

$$\begin{aligned}&[I_0(\lambda)\hat{M}_{AC0}(\lambda) - J_0(\lambda)\hat{M}_{CC0}(\lambda)][I_p(\lambda)\hat{M}_{ACp}(\lambda) - J_p(\lambda)\hat{M}_{CCp}(\lambda)]\\ &-[I_0(\lambda)\hat{\Omega}_{AC0}(\lambda) - J_0(\lambda)\hat{\Omega}_{CC0}(\lambda)][I_p(\lambda)\hat{\Omega}_{ACp}(\lambda) - J_p(\lambda)\hat{\Omega}_{CCp}(\lambda)] = 0\end{aligned}\,. \tag{28}$$

The solution of the above equation gives rise to the eigenvalues λ_{sm} and their mode shape functions:

$$\phi_{sm}(\vec{\sigma}) = \hat{R}_{C0}(\frac{\lambda_{sm}}{a}r) + \cos(p\theta)\hat{R}_{Cp}(\frac{\lambda_{sm}}{a}r)\,, \tag{29}$$

where

$$\hat{R}_{C0}(\frac{\lambda_{sm}}{a}r)=[J_0(\frac{\lambda_{sm}}{a}r)-\frac{J_0(\lambda_{sm})}{I_0(\lambda_{sm})}I_0(\frac{\lambda_{sm}}{a}r)] \quad \text{and} \tag{30a}$$

$$\hat{R}_{Cp}(\frac{\lambda_{sm}}{a}r)=\frac{[\hat{\Omega}_{AC0}(\lambda_{sm})-\frac{J_0(\lambda_{sm})}{I_0(\lambda_{sm})}\hat{\Omega}_{CC0}(\lambda_{sm})]}{[\hat{M}_{ACp}(\lambda_{sm})-\frac{J_p(\lambda_{sm})}{I_p(\lambda_{sm})}\hat{M}_{CCp}(\lambda_{sm})]}[J_p(\frac{\lambda_{sm}}{a}r)-\frac{J_p(\lambda_{sm})}{I_p(\lambda_{sm})}I_p(\frac{\lambda_{sm}}{a}r)]. \tag{30b}$$

3.2 Results and Discussion

The above modal characteristics are illustrated by the natural frequencies and mode shapes of the first three circumferential modes, $(s,m)=(0,1),(1,1)_C,(1,1)_S$, in a steel circular plate ($E=21\times10^{10}\,\mathrm{N/m^2}$, $\nu=0.3$ $\rho=7.8\times10^3\,\mathrm{kg/m^3}$) with $h=0.003\mathrm{m}$ and $a=0.206\mathrm{m}$. The natural frequencies of the (0,1) and (1,1) modes of the plate with clamped boundary conditions are $f_{(0,1)}=180\mathrm{Hz}$ and $f_{(1,1)_C}=f_{(1,1)_S}=376\mathrm{Hz}$ respectively. If the boundary is supported by a uniform torsional stiffness with stiffness ratio of $S_R=5$, the natural frequencies reduce $f_{(0,1)}=140\mathrm{Hz}$ and $f_{(1,1)_C}=f_{(1,1)_S}=305\mathrm{Hz}$ due to the reduced boundary stiffness. The maximum amplitude points of the $(1,1)_C$ and $(1,1)_S$ modes shift closer to the boundary as shown in Figure 2(a). If the boundary stiffness ratio is $S_R=5+3\cos(\theta)$, $(0,1)$ and $(1,1)_C$ modes are coupled due to the stiffness component $S_{RC1}=3\cos(\theta)$. The natural frequencies of the coupled modes are $f_{[(0,1)+(1,1)_C]_1}=137\mathrm{Hz}$ and $f_{[(0,1)+(1,1)_C]_2}=303\mathrm{Hz}$. The corresponding mode shapes are the superposition of that of the $(0,1)$ and $(1,1)_C$ modes and shown in Figure 2(b), where $[(0,1)+(1,1)_C]_1$ mode is dominated by the $(0,1)$ mode, and $[(0,1)+(1,1)_C]_2$ by the $(1,1)_C$ mode. However, natural frequency and mode shape of the $(1,1)_S$ mode are not affected by the boundary stiffness S_{RC1} and thus remain as described in Figure 2(b). As a result, splitting in natural frequencies occurs in the original degenerate $(1,1)_C$ and $(1,1)_S$ modes. Figure 3 shows the normalized natural frequencies of the first three modes as a function of stiffness ratio of the uniform torsional spring at the boundary. The solid black and red curves are the normalized natural frequencies of $(0,1)$, $(1,1)_C$ and $(1,1)_S$ modes when $S_{RC1}=0$ (without the coupling between $(0,1)$ and $(1,1)_C$). Without the coupling, $(1,1)_C$ and $(1,1)_S$ modes are degenerate, and they have the same natural frequency curve (red). As the stiffness ratio S_{RC0} decreases, the natural frequencies decrease compared to those of a clamped plate due to reduced constraint on the angular displacement at the boundary. If an extra stiffness ratio $S_{RC1}=3$ is present, the coupling between the $(0,1)$ and $(1,1)_C$ modes further reduces the constraint on the boundary angular displacement, resulting in a further decrease in natural frequencies of the $(0,1)$ dominated (solid blue) and $(1,1)_C$ dominated (dotted blue) modes. Meanwhile the natural frequency of the $(1,1)_S$ is still represented by the red curve in Figure 3.

(a)

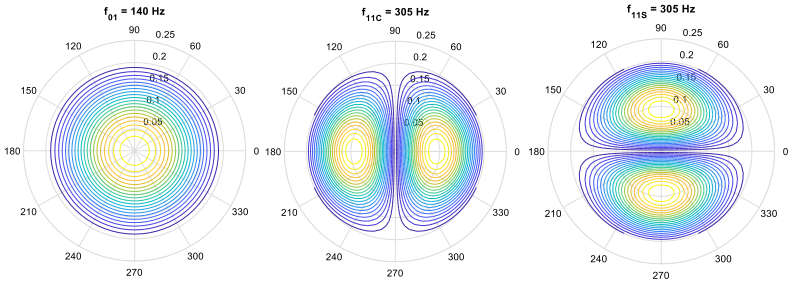

(b)

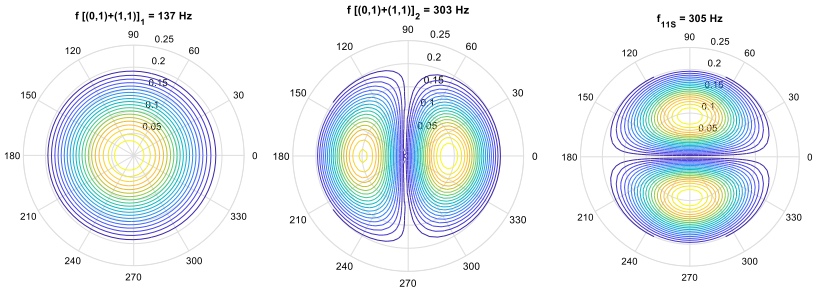

Figure 2 – Shapes and natural frequencies of the first three modes of the plate, (a) $S_R = 5$ *and (b)* $S_R = 5 + 3\cos(\theta)$.

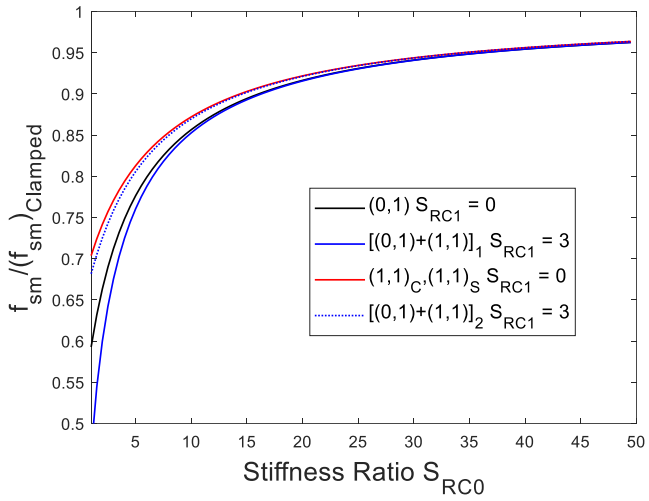

Figure 3 – Normalized natural frequencies of the first three circumferential modes in the plate.

It is worth noting that the theoretical model used in this analysis originates from a circular plate supported by flanges. Twelve evenly distributed bolts on the flange apply clamping force to constrain both the transverse and angular displacements at the interface between the plate and flange. Due to the distributed nature of the flange and clamping forces, the model, shown in Figure 1, should be extended to represent the distributed flange. Additionally, it accounts for the distributed transverse and torsional stiffness arising from the non-uniform clamping forces between the flange and plate, caused by the locally tensioned bolts. A preliminary comparison of the drive point accelerance between measured results and Comsol simulations indicates that the transverse stiffness due to the bolts' clamping is approximately $1.46\times10^{10}\,\mathrm{N/m}$.

4 CONCLUSIONS

The characteristics of coupled circumferential modes in a circular plate are derived and summarised as follows:

(1) If the boundary of a circular plate is supported by a uniform torsional boundary stiffness $K_{\psi C0}$, the circumferential modes are uncoupled. The natural frequency of each mode reduces when boundary conditions are less restrictive than perfect clamping. The cosine and sine components of the same circumferential modal number are degenerate modes, meaning they share the same natural frequency and will experience the same frequency shift for a given $K_{\psi C0}$. As the stiffness ratio increases, the natural frequencies of all the plate modes approach those of a perfectly clamped plate.

(2) If a non-uniform boundary stiffness component, $K_{\psi Cp}\cos(p\theta)$ for $p \neq 0$, is superimposed to the uniform stiffness, the $s = 0$ and $s = p$ cosine modes are coupled, resulting split of the natural frequencies of otherwise degenerated $\cos(p\theta)$ and $\sin(p\theta)$ modes. Furthermore, both the $s = 0$ and $s = p$ cosine modes are in presence of the shapes of the coupled ($s = 0$, $s = p$) circumferential modes.

REFERENCES

Terwagne, D. & Bush, J. W. M. (2011). *Tibetan singing bowls*, Nonlinearity, 24 (2011) R51–R66.

Sheldrake, M. & Sheldrake, R. (2017). *Determinants of Faraday wave-patterns in water samples oscillated vertically at a range of frequencies from 50-200 Hz*, WATER, 2017,1-27.

Xu, P. & Wellens, P. (2021). *Effects of static loads on the nonlinear vibration of circular plates*, Journal of Sound and Vibration 504, 2021, 1-17.

Alekseev, V. V., IndeÏtsev, D. A. & Mochalova, Y. A. (2002). *Vibration of a flexible plate in contact with the free surface of a heavy liquid*, Technical Physics, Vol. 47, No. 5, 2002, 529–534.

Matthews, D., Sun, H., Saltmarsh, K., Wilkes, D., Munyard A. & Pan, J. (2014). *A detailed experimental modal analysis of a clamped circular plate*, Inter-noise 2014, Melbourne, Australia.

Leissa, A. (1993). Vibration of Plates. Acoustical Society of America.

APPENDIX

For the uniform stiffness component, $p = 0$,

$$\Pi_{C0}^{ns} = \begin{bmatrix} \Lambda_{Cns} & 0 \\ 0 & \Lambda_{Sns} \end{bmatrix},\ \Pi_{S0}^{ns} = 0 \text{ where } \Lambda_{Cns} = \begin{cases} \pi & n = s \neq 0 \\ 2\pi & n = s = 0 \\ 0 & n \neq s \end{cases} \text{ and } \Lambda_{Sns} = \begin{cases} \pi & n = s \neq 0 \\ 0 & n = s = 0 \\ 0 & n \neq s \end{cases}. \quad \text{(A1)}$$

If $p \neq 0$, the non-zero elements in Equations (9) and (10) are:

$$\Pi_{Cp}^{ns}(1,1) = \int_0^{2\pi} \cos(n\theta)\cos(s\theta)\cos(p\theta)d\theta = \begin{cases} \pi & (s = p \neq 0, n = 0), (s = 0, n = p \neq 0) \\ 0 & otherwise \end{cases}, \quad \text{(A2a)}$$

$$\Pi_{Sp}^{ns}(1,2) = \int_0^{2\pi} \cos(n\theta)\sin(s\theta)\sin(p\theta)d\theta = \begin{cases} \pi & (s = p \neq 0, n = 0) \\ 0 & otherwise \end{cases} \text{ and} \quad \text{(A2b)}$$

$$\Pi_{Sp}^{ns}(2,1) = \int_0^{2\pi} \sin(n\theta)\cos(s\theta)\sin(p\theta)d\theta = \begin{cases} \pi & (s = 0, p = n \neq 0) \\ 0 & otherwise \end{cases}. \quad \text{(A2c)}$$